

Geodesics of electrically and magnetically charged test particles in the Reissner-Nordström space-time: analytical solutions

Saskia Grunau and Valeria Kagramanova

Institut für Physik, Universität Oldenburg, D-26111 Oldenburg, Germany

November 25, 2010

Abstract

We present the full set of analytical solutions of the geodesic equations of charged test particles in the Reissner-Nordström space-time in terms of the Weierstraß \wp , σ and ζ elliptic functions. Based on the study of the polynomials in the ϑ and r equations we characterize the motion of test particles and discuss their properties. The motion of charged test particles in the Reissner-Nordström space-time is compared with the motion of neutral test particles in the field of a gravitomagnetic monopole. Electrically or magnetically charged particles in the Reissner-Nordström space-time with magnetic or electric charges, respectively, move on cones similar to neutral test particles in the Taub-NUT space-times.

1 Introduction

The Reissner-Nordström space-time is a static, asymptotically flat solution of the Einstein-Maxwell equations in general relativity. It describes charged, non-rotating spherical black holes or naked singularities. In general, the Reissner-Nordström space-time represents a gravitating source which is both electrically and magnetically charged. It is a special case of the general family of electrovacuum space-times of Petrov type D found by Plebański and Demiański [1] and reviewed by Griffiths and Podolský [2]. These space-times describe the gravitational fields of isolated massive objects, e.g. stars or black holes, and are in addition characterized by a NUT charge, angular momentum, acceleration and a cosmological constant. The higher dimensional generalizations of the Reissner-Nordström solution were found by Tangherlini [3].

The physical properties of a space-time can be investigated by studying the motion of test particles and light in this space-time. Test particles are a sensitive tool to investigate the properties of the fields generated by the massive body because of the coupling of the parameters of the metric and the test particle in the equations of motion. The geodesic equations can be solved either analytically or numerically. A pioneer in finding analytical solutions was Hagihara [4]. He integrated the geodesic equation of a test particle in the Schwarzschild gravitational field in terms of the Weierstrass \wp -function. Some special cases of the geodesics in the Reissner-Nordström space-time were studied in [5, 6]. General features of the motion of charged test particles in the Kerr-Newman space-time were considered in [7]. The influence of the gravitomagnetic monopole moment on the motion of test particles in Kerr-Newman-Taub-NUT space-time was studied in [8].

A breakthrough in the analytical integration of geodesics came with the papers of Hackmann and Lämmerzahl [9, 10] where geodesics in a 4-dimensional Schwarzschild-de Sitter space-time were integrated analytically in terms of the hyperelliptic θ and σ functions. The developed method is based on the Jacobi inversion problem restricted to the θ -divisor. Also geodesics in the Reissner-Nordström-de Sitter space-time in 4 dimensions as well as in some higher dimensional Schwarzschild, Schwarzschild-(anti)de Sitter, Reissner-Nordström and Reissner-Nordström-(anti)de Sitter space-times were integrated by this mathematical method [11]. The elliptic and hyperelliptic functions were subsequently used to obtain the solutions of the geodesic equations in the axially symmetric Taub-NUT [12] and Kerr-de Sitter [13] space-times. In these papers the types of orbits are classified and the orbits of test particles are extensively studied. Furthermore, the analytical solution of the geodesic equations in the general Plebański-Demiański space-time in 4 dimensions were obtained in terms of the hyperelliptic Kleinian σ function [14].

The Reissner-Nordström space-time as well as the Schwarzschild space-time have singularities at their origin. Whereas in the Schwarzschild space-time particles are bound to end up in the central singularity,

this does not hold for particles which cross the event horizon in the charged space-time. Here the potential barrier due to the charge does not allow the singularity to swallow the particles. Instead, a (test) particle will leave the vicinity of the singularity again. After traversing the Cauchy horizon and the event horizon of the Reissner-Nordström black hole, the particle will emerge in another universe [5, 15, 11]. Moreover, an orbit in such a black hole space-time can be analytically continued into an infinite sequence of further patches of the space-time. This feature of the Reissner-Nordström solution is seen clearly in its Carter-Penrose diagram.

The Taub-NUT space-time which is characterized by a gravitomagnetic charge possesses also two horizons. A Kruskal-like analytic extension [16] of the Taub-NUT space-time would then likewise allow test particles to move into other worlds. However, such an extension comes at the prize that the periodic identification of the time coordinate, suggested by Misner to remove the singularity from the symmetry axis, is no longer possible [16]. Consequently, the space-time is geodesically incomplete, since orbits end either at the singular axis (in the Bonnor-Manko-Ruiz interpretation) or at one of the horizons (in the Misner-Taub interpretation). For a recent discussion see [12].

But the presence of two horizons and the associated many-world orbits is not the only similarity between the Reissner-Nordström space-time with electromagnetic charge and the Taub-NUT space-time with gravitomagnetic charge. Also the motion of test particles has common properties in both types of space-times. In this paper we study the motion of electrically and/or magnetically charged particles in the general Reissner-Nordström space-time. As in the Taub-NUT spacetime where a test particle moves on a cone, the motion of a charged test particle in the general Reissner-Nordström space-time proceeds on a cone. The condition for the motion on a cone is that the products of the dual charges should not be equal i.e., $Gq \neq Qg$ (where Q and G are the electric and magnetic charges of the gravitational source and q and g those of the test particle, see Section 2 for details). Otherwise the motion would be planar.

In the following section we present the equations of motion. We classify the orbits of charged test particles in Section 3. We analyze their motion by studying the influence of the parameters of the metric and of the test particles. In particular, we consider the dependence on the mass, on the angular momentum, on the charges and on the separation (Carter) constant. In Section 4 we solve analytically the r , ϑ , φ and t equations of motion, and we give the solutions of the radial and time equations in terms of the Weierstrass elliptic \wp , σ and ζ functions. We give details on the elliptic integrals in the Appendices.

2 The geodesic equation

The Reissner-Nordström solution of the Einstein-Maxwell field equations is described by the metric [2]

$$ds^2 = \frac{\Delta_r}{r^2} dt^2 - \frac{r^2}{\Delta_r} dr^2 - r^2 (d\vartheta^2 + \sin^2 \vartheta d\varphi^2), \quad (1)$$

where $\Delta_r = r^2 - 2Mr + Q^2 + G^2$. Here M is the mass of the solution, Q and G are the electric and magnetic charges. The singularity is located at $r = 0$. For $0 < Q^2 + G^2 < M^2$, there are two horizons, defined by $\Delta_r = 0$, and given by

$$r_{\pm} = M \left(1 \pm \sqrt{M^2 - (Q^2 + G^2)} \right). \quad (2)$$

Between the horizons the radial coordinate r becomes timelike, and the time coordinate t spacelike. When $Q^2 + G^2 = M^2$, the horizons degenerate and the black hole is called extremal. For $Q^2 + G^2 > M^2$ the solution has a naked singularity.

The field strength $F_{\mu\nu} = A_{\nu,\mu} - A_{\mu,\nu}$ and the dual field strength $\check{F}_{\mu\nu} = \check{A}_{\nu,\mu} - \check{A}_{\mu,\nu}$ of the electromagnetic field are induced by the non-vanishing components of the vector potentials A_μ and \check{A}_μ

$$A_t = \frac{Q}{r}, \quad A_\varphi = -G \cos \vartheta, \quad (3)$$

$$\check{A}_t = i \frac{G}{r}, \quad \check{A}_\varphi = iQ \cos \vartheta. \quad (4)$$

The dual field strength is defined by the antisymmetric Levi-Civita symbol $\varepsilon^{\mu\nu\sigma\tau}$ as $\check{F}^{\mu\nu} = \frac{i}{2\sqrt{g^d}} \varepsilon^{\mu\nu\sigma\tau} F_{\sigma\tau}$ with $g^d = -\det||g_{\mu\nu}||$.

The Hamilton-Jacobi equation for a particle with electric charge q and magnetic charge g

$$2\frac{\partial S}{\partial \tau} = g^{\mu\nu} \left(\frac{\partial S}{\partial x^\mu} - qA_\mu + ig\check{A}_\mu \right) \left(\frac{\partial S}{\partial x^\nu} - qA_\nu + ig\check{A}_\nu \right) \quad (5)$$

has a solution in the form $S = \frac{1}{2}\delta\tau - Et + L\varphi + S(r) + S(\vartheta)$. Here τ is an affine parameter along the geodesic, δ is a parameter which is equal to 0 for a massless test particle and equal to 1 for a test particle with non-zero mass. The constants E and L are the conserved energy and the angular momentum in the z direction of a test particle, respectively. Because of the presence of the angle dependent terms qA_φ and $g\check{A}_\varphi$ in (5) the problem of charged particle motion is axially symmetric, although the space-time itself as described by the metric (1) is spherically symmetric.

For convenience, we introduce dimensionless quantities ($r_S = 2M$)

$$\tilde{r} = \frac{r}{r_S}, \quad \tilde{t} = \frac{t}{r_S}, \quad \tilde{\tau} = \frac{\tau}{r_S}, \quad \tilde{Q} = \frac{Q}{r_S}, \quad \tilde{G} = \frac{G}{r_S}, \quad \tilde{L} = \frac{L}{r_S}. \quad (6)$$

The Hamilton-Jacobi equation (5) separates and yields for each coordinate a corresponding differential equation

$$\left(\frac{d\tilde{r}}{d\gamma} \right)^2 = R \quad (7)$$

$$\left(\frac{d\vartheta}{d\gamma} \right)^2 = \Theta \quad (8)$$

$$\frac{d\varphi}{d\gamma} = \frac{1}{\sin^2 \vartheta} (\tilde{L} + \Delta_g \cos \vartheta) \quad (9)$$

$$\frac{d\tilde{t}}{d\gamma} = \frac{\tilde{r}^4}{\tilde{\Delta}_r} \left(E + \frac{\Delta_q}{\tilde{r}} \right), \quad (10)$$

with the polynomial R and the function Θ

$$R = \tilde{r}^4 \left(E + \frac{\Delta_q}{\tilde{r}} \right)^2 - \tilde{\Delta}_r (\delta\tilde{r}^2 + k) \quad (11)$$

$$\Theta = k - \frac{1}{\sin^2 \vartheta} (\tilde{L} + \Delta_g \cos \vartheta)^2. \quad (12)$$

The following notations were introduced: $\Delta_g = \tilde{G}q - \tilde{Q}g$, $\Delta_q = \tilde{Q}q + \tilde{G}g$ and $\tilde{\Delta}_r = \tilde{r}^2 - \tilde{r} + \tilde{Q}^2 + \tilde{G}^2$. Here $k = K + \tilde{L}^2$, where K is known as Carter constant or separation constant. For zero charges the equations of motion above reduce to the Schwarzschild case. We also used the Mino time γ as $\tilde{r}^2 d\gamma = d\tilde{\tau}$ [17]. Note, that for $\Delta_g = 0$ the situation simplifies, and the motion takes place in a plane.

3 Complete classification of geodesics

Consider the Hamilton-Jacobi equations (7)-(10). The properties of the orbits are given by the polynomial R (11) and the function Θ (12). The constants of motion (energy, angular momentum and separation constant) as well as the parameters of the metric and the charges of the test particle characterize these polynomials and, as a consequence, the types of orbits. In this section we discuss the charged motion in the Reissner-Nordström space-times in terms of the properties of the underlying polynomial R and the function Θ .

3.1 The ϑ -motion

Since ϑ is a polar angle, it can take only real values. Equation (8) has real solutions if the requirement $\Theta \geq 0$ is fulfilled. This implies $k \geq 0$. With the new variable $\xi = \cos \vartheta$, Eq. (8) turns into the equation

$$\left(\frac{d\xi}{d\gamma} \right)^2 = \Theta_\xi \quad \text{with} \quad \Theta_\xi = a\xi^2 + b\xi + c, \quad (13)$$

with a simple polynomial of second order on the right hand side, where $a = -(k + \Delta_g^2)$, $b = -2\tilde{L}\Delta_g$, and $c = k - \tilde{L}^2$. From $k \geq 0$ follows $a < 0$. The zeros of Θ_ξ define the angles of two cones which confine

the motion of the test particles (a similar feature appears in Taub-NUT [12] and Kerr space-times [13]). Moreover, every trajectory is not only constrained by these cones but lies itself on a cone in 3-space [18, 19]. If Δ_g in the equation (9) and in the polynomial (12) vanishes, then the motion lies on a plane (e.g., the motion of only electrically charged or neutral particles reduces to a plane in a Reissner-Nordström space-time with only electric charge). In the space-time of a gravitomagnetic monopole the trajectories of test particles similarly lie on cones [20, 21, 22].

The discriminant $D = b^2 - 4ac$ of the polynomial Θ_ξ can be written as $D = 4k\kappa$ with $\kappa = k + \Delta_g^2 - \tilde{L}^2$. The existence of real zeros of Θ_ξ requires $D \geq 0$. This implies that both k and κ should be non-negative

$$\begin{aligned} k &\geq 0 \\ \kappa = k - \tilde{L}^2 + \Delta_g^2 &\geq 0. \end{aligned} \quad (14)$$

These are conditions on the parameters \tilde{L} and k for given values of \tilde{Q} , \tilde{G} , q and g . As long as $k - \tilde{L}^2$ is positive there are no constraints on \tilde{L} . When $k - \tilde{L}^2$ becomes negative the inequalities (14) imply a lower limit for the angular momentum given by $\tilde{L}_{\min} = \pm\sqrt{\Delta_g^2 + k}$.

One can show that

$$\Theta = k - \frac{1}{\sin^2 \vartheta} (\tilde{L} + \cos \vartheta \Delta_g)^2 = \kappa - \frac{1}{\sin^2 \vartheta} (\tilde{L} \cos \vartheta + \Delta_g)^2. \quad (15)$$

The zeros of Θ_ξ are given by

$$\xi_{1,2} = \frac{\tilde{L}\Delta_g \pm \sqrt{k\kappa}}{-(k + \Delta_g^2)}. \quad (16)$$

The conditions (14) ensure the compatibility of $\xi \in [-1, 1]$ with $\Theta_\xi \geq 0$.

The function Θ_ξ describes a parabola with the maximum at $\left(-\frac{\tilde{L}\Delta_g}{k + \Delta_g^2}, \frac{k\kappa}{k + \Delta_g^2}\right)$. For non-vanishing \tilde{L} and Δ_g the maximum of the parabola is no longer located at $\xi = 0$ or, equivalently, the zeros are no longer symmetric with respect to $\xi = 0$. Only for vanishing \tilde{L} or Δ_g both cones are symmetric with respect to the equatorial plane.

The ϑ -motion can be classified according to the sign of $k - \tilde{L}^2$:

1. If $k - \tilde{L}^2 < 0$ then Θ_ξ has 2 positive zeros for $\tilde{L}\Delta_g < 0$ and $\vartheta \in (0, \pi/2)$, so that the particle moves above the equatorial plane without crossing it. If $\tilde{L}\Delta_g > 0$ then $\vartheta \in (\pi/2, \pi)$.
2. If $k - \tilde{L}^2 = 0$ then Θ_ξ has two zeros: $\xi_1 = 0$ and $\xi_2 = -\frac{2\tilde{L}\Delta_g}{\tilde{L}^2 + \Delta_g^2}$. If $\tilde{L}\Delta_g < 0$ then $\xi \in [0, 1)$ and $\vartheta \in (0, \frac{\pi}{2}]$. If $\tilde{L}\Delta_g > 0$ then $\xi \in (-1, 0]$ and $\vartheta \in [\frac{\pi}{2}, \pi)$. If $\tilde{L} = -\Delta_g$ then the ϑ -motion fills the whole upper hemisphere $\vartheta \in [0, \frac{\pi}{2}]$. The motion fills the whole lower hemisphere with $\vartheta \in [\frac{\pi}{2}, \pi]$ if $\tilde{L} = \Delta_g$.
3. If $k - \tilde{L}^2 > 0$ then Θ_ξ has a positive and a negative zero and $\vartheta \in (0, \pi)$, and the particle crosses the equatorial plane during its motion.

In general, the second term of the function Θ in (15) diverges for $\vartheta \rightarrow 0, \pi$. However, if $\tilde{L} = -\Delta_g$ this term is regular for $\vartheta = 0$ and if $\tilde{L} = \Delta_g$ it is regular for $\vartheta = \pi$. If $\tilde{L} = \pm\Delta_g$, then $k = \kappa$. The regularity of Θ in these cases can be seen from

$$\Theta = \kappa - \tilde{L}^2 \frac{(1 \mp \cos \vartheta)^2}{\sin^2 \vartheta}, \quad (17)$$

by application of L'Hôpital's rule. If, furthermore, $\tilde{L}^2 = 0$ then $\Theta = k + \Delta_g^2 - \tilde{L}^2$ which is independent of ϑ .

In the special cases when one of the constants k or κ or both vanish, Θ_ξ has a double root which is the only possible value for ϑ . One can distinguish three cases:

1. If $k = 0$ and $\kappa > 0$, then $\xi = -\frac{\tilde{L}}{\Delta_g}$ for $\tilde{L}^2 < \Delta_g^2$.
2. If $\kappa = 0$ and $k > 0$ then $\xi = -\frac{\Delta_g}{\tilde{L}}$ for $\tilde{L}^2 > \Delta_g^2$.

3. If $k = \kappa = 0$ then $\xi = \pm 1$ implying that $\vartheta = 0$ or $\vartheta = \pi$ are possible. In this case $\tilde{L} = \mp\Delta_g$ (as discussed above).

This means that during a test particle's motion the coordinate ϑ is constant and the trajectory lies on a cone around the $\vartheta = 0, \pi$ -axis with the opening angle $\arccos\xi$. In this case we immediately obtain from (9) that $\varphi(\gamma) = \mathcal{C}(\gamma - \gamma_{\text{in}})$ with a constant $\mathcal{C} = \frac{\tilde{L} + \xi\Delta_g}{1 - \xi^2}$ which in case 1 is $\mathcal{C} = 0$ and in case 2 is $\mathcal{C} = \tilde{L}$.

Thus, the non-vanishing of k and κ indicates that the motion of the particle is not symmetric with respect to the $\vartheta = 0, \pi$ -axis. Therefore, these two constants may be regarded to play the role of a generalized Carter constant which appears, e.g., in the motion of particles in NUT and Kerr space-times.

3.2 The \tilde{r} -motion

3.2.1 Possible types of orbits

In the following we consider the motion of charged particles in the regular Reissner-Nordström black hole space-time, possessing two non-degenerate horizons r_{\pm} . Before discussing the \tilde{r} -motion in detail, we introduce a list of all possible orbits:

1. *Escape orbits* (EO) with ranges: (r_1, ∞) with $r_1 > r_+$. These escape orbits do not cross the horizons.
2. *Two-world escape orbits* (TEO) with ranges (r_1, ∞) with $r_1 < r_-$
3. *Periodic bound orbits* (BO) with range $\tilde{r} \in (r_1, r_2)$ with $r_1 < r_2$ and
 - (a) either $r_1, r_2 > r_+$ or
 - (b) $r_1, r_2 < r_-$.
4. *Many-world periodic bound orbits* (MBO) with range $\tilde{r} \in (r_1, r_2)$ where $r_1 < r_-$ and $r_2 > r_+$.

Here we used the notation for the orbits introduced in [11] for the regular Reissner-Nordström space-time.

3.2.2 The radial motion

The right hand side of the differential equation (7) has the form $R = \sum_{i=0}^4 b_i \tilde{r}^i$ with the coefficients

$$b_4 = E^2 - \delta \quad (18)$$

$$b_3 = \delta + 2E\Delta_q \quad (19)$$

$$b_2 = -(k - \Delta_q^2 + \delta(\tilde{Q}^2 + \tilde{G}^2)) \quad (20)$$

$$b_1 = k \quad (21)$$

$$b_0 = -k(\tilde{Q}^2 + \tilde{G}^2). \quad (22)$$

Let us now consider massive particles only, that is $\delta = 1$. In order to obtain real values for \tilde{r} from (7) we have to require $R \geq 0$. The regions for which $R \geq 0$ are bounded by the zeros of R . The number of zeros depends on the values of E , k , \tilde{Q} , \tilde{G} , q and g . Two conditions $R = 0$ and $\frac{dR}{d\tilde{r}} = 0$ define the double zeros of the polynomial R and thereby the boundary between the regions where R has 1, 2, 3 or 4 zeros. The parameter plots shown in Fig. 1 are based on this. One has to additionally take care of the change of the sign of $E^2 - 1$ when E crosses $E^2 = 1$. Then the sign of $R(\tilde{r})$ for $\tilde{r} \rightarrow \pm\infty$ changes. Furthermore, the case $E^2 = 1$ requires additional attention: If the line $E^2 = 1$ is contained in a region with 3 or 1 zeros then on this portion of the line we have 3 or 1 zeros respectively. Taking all these features into account we obtain the k - E diagrams of Fig. 1.

We define the effective potential from equation (7) as the values of energy E when

$$0 = \left(\frac{d\tilde{r}}{d\gamma} \right)^2 = \tilde{r}^4(E - V_{\text{eff}}^+)(E - V_{\text{eff}}^-), \quad (23)$$

thus,

$$V_{\text{eff}}^{\pm} = -\frac{\Delta_q}{\tilde{r}} \pm \frac{1}{\tilde{r}^2} \sqrt{\tilde{\Delta}_r(\delta\tilde{r}^2 + k)}. \quad (24)$$

Condition (23) then determines the turning points of an orbit.

Examples for the effective potential are given in Figs. 2, 3. These figures combine the positive-root part V_{eff}^+ and the negative-root part V_{eff}^- . At the horizons both parts V_{eff}^{\pm} coincide (i.e. at these points

both parts V_{eff}^\pm are glued together), since $\tilde{\Delta}_r$ vanishes here. Consequently, $V_{\text{eff}}^\pm(r_\pm) = -\frac{\Delta_q}{r_\pm}$. Clearly, $V_{\text{eff}}^\pm(r_\pm) < 0$ if $\Delta_q > 0$ and vice versa (see e.g. Fig.3).

We note, that in contrast to the Schwarzschild case here the positive-root V_{eff}^+ can allow for particles with negative energies. The region outside the horizon where negative energy particles may sojourn has been termed ‘generalized ergosphere’, since energy may be extracted [23, 24]. While particle energies below the negative-root V_{eff}^- have no classical interpretation, they are associated with antiparticles in the framework of quantum field theory [25]. The relation $V_{\text{eff}}^+(E, q, g) = -V_{\text{eff}}^-(E, -q, -g)$ shows, that the corresponding positive energy orbits are available for particles with opposite charges (i.e., antiparticles). A lower limit for the energies of particles is obtained from the requirement that time should only run forward (see Eq. (10)), $E \geq -\frac{\Delta_q}{r}$.

As we know from previous studies for neutral particles (see e.g. [11]), the Reissner-Norström space-time possesses a potential barrier which prevents particles from falling into the singularity. The potential barrier which is defined by the smallest positive root r_1 of R is located in the interval $0 < r_1 \leq r_-$.

For increasing values of Δ_q , the influence of the charge of a test particle becomes noticeable through the term $-\frac{\Delta_q}{r}$. (We recall, that the charges of the black hole \tilde{Q} and \tilde{G} are constrained by the naked singularity condition $\tilde{Q}^2 + \tilde{G}^2 > \frac{1}{4}$). Namely, for larger values of the test particle charge the effective potential can form a small potential mound (Fig.3(a)) or potential well (Fig.3(b)) in the interval $(0, r_-]$. This indicates that bound orbits may exist in this region. Such a feature is only present in the motion of charged particles.

Using the k - E diagrams in Fig. 1 as well as the above considerations we can give all possible combinations of zeros of R and an interpretation in terms of specific types of orbits which are summarized in Table 1.

The types of orbits related to the various parameters are given by:

- Region (1): one positive zero. The orbit is a TEO with particles coming from $\tilde{r} = +\infty$. From the features of the effective potential (potential barrier) it is clear that the turning point can lie on the inner horizon (case A_-). In this case the energy of a test particle corresponds to the glue point of the potentials V_{eff}^\pm : $E_{A_-} = V_{\text{eff}}^\pm(r_-)$. For $E^2 = 1$ the coefficient of the highest power in R , given by $E^2 - 1$ for massive test particles, vanishes. On the line $E^2 = 1$ within the region (1) there is one positive zero.
- Region (2): two positive zeros. Here only MBOs are possible. In the special case when $\Delta_q = 0$ and $E^2 = 0$, the turning points are lying on the horizons (case B_\pm). Also the cases B_- and B_+ when one of the turning points lies on the horizons are possible. In this case the energy again corresponds to the glue points of the potentials V_{eff}^\pm : $E_{B_-} = V_{\text{eff}}^\pm(r_-)$ (such an orbit can be found in e.g. Fig.2(a)) or $E_{B_+} = V_{\text{eff}}^\pm(r_+)$ (see e.g. Fig.3(b)) respectively.
- Region (3): three positive zeros.
 - Region (3)₊: Here MBOs and EOs with corresponding subcases C_- and C_+ are possible.
 - Region (3)₋: For growing charges the term $-\frac{\Delta_q}{r}$ leads to a bound orbit with turning points behind the inner horizon. It is also possible that a turning point of the TEO lies on the inner horizon (case D_-).

Here too for $E^2 = 1$ the term of highest power in R vanishes giving three positive zeros for the $E^2 = 1$ -line within the region (3).

- Region (4): four positive zeros. Here we find MBOs and BOs (planetary orbits).

4 Solution of the geodesic equation

Now we present the analytical solutions of the differential equations (7)–(10).

4.1 Solution of the ϑ -equation

The solution of Eq. (13) with $a < 0$ and $D > 0$ is given by the elementary function

$$\vartheta(\gamma) = \arccos\left(\frac{1}{2a}\left(\sqrt{D}\sin\left(\sqrt{-a}\gamma - \gamma_{\text{in}}^\vartheta\right) - b\right)\right), \quad (25)$$

type	region	+zeros	range of \tilde{r}	orbit
A	(1)	1		TEO
A ₋				TEO ₋
B	(2)	2		MBO
B ₊				MBO ₊
B ₋				MBO ₋
B _±				MBO _±
C	(3) ₊	3		MBO, EO
C ₋				MBO, EO
C ₊				MBO ₊ , EO
D	(3) ₋	3		BO, TEO
D ₋				BO, TEO
E	(4)	4		MBO, BO

Table 1: Types of polynomials and orbits of charged particles in the Reissner-Nordström space-time. The thick lines represent the range of the orbits. The turning points are shown by thick dots. The horizons are indicated by a vertical double line. In special cases the turning points lie on the horizons. Type D with a bound orbit behind the inner horizon is possible for charged particles with relatively large charges.

where $\gamma_{\text{in}}^\vartheta = \sqrt{-a}\gamma_{\text{in}} - \arcsin\left(\frac{2a\xi_{\text{in}}+b}{\sqrt{b^2-4ac}}\right)$ and γ_{in} is the initial value of γ .

4.2 Solution of the \tilde{r} -equation

For timelike geodesics the polynomial R in (11) is of fourth order. A standard substitution $\tilde{r} = \pm\frac{1}{x} + \tilde{r}_R$, where \tilde{r}_R is a zero of R , reduces (7) to a differential equation with a third order polynomial $\left(\frac{dx}{d\gamma}\right)^2 = R_3$, where $R_3 = \sum_{i=0}^3 b_i x^i$. A further substitution $x = \frac{1}{b_3}(4y - \frac{b_2}{3})$ transforms that into the standard Weierstraß form

$$\left(\frac{dy}{d\gamma}\right)^2 = 4y^3 - g_2 y - g_3 = P_3(y), \quad (26)$$

where

$$g_2 = \frac{b_2^2}{12} - \frac{b_1 b_3}{4}, \quad g_3 = \frac{b_1 b_2 b_3}{48} - \frac{b_0 b_3^2}{16} - \frac{b_2^3}{216}. \quad (27)$$

The differential equation (26) is of elliptic type and is solved by the Weierstraß \wp -function [26]

$$y(\gamma) = \wp(\gamma - \gamma'_{\text{in}}; g_2, g_3), \quad (28)$$

where $\gamma'_{\text{in}} = \gamma_{\text{in}} + \int_{y_{\text{in}}}^{\infty} \frac{dy}{\sqrt{4y^3 - g_2 y - g_3}}$ with $y_{\text{in}} = \pm\frac{b_3}{4}(\tilde{r}_{\text{in}} - \tilde{r}_R)^{-1} + \frac{b_2}{12}$. Then the solution of (7) acquires the form

$$\tilde{r} = \pm \frac{b_3}{4\wp(\gamma - \gamma'_{\text{in}}; g_2, g_3) - \frac{b_2}{3}} + \tilde{r}_R. \quad (29)$$

4.3 Solution of the φ -equation

Eq. (9) can be simplified by using (8) and by performing the substitution $\xi = \cos \vartheta$

$$d\varphi = -\frac{d\xi}{\sqrt{\Theta_\xi}} \frac{\tilde{L}}{1-\xi^2} - \frac{\xi d\xi}{\sqrt{\Theta_\xi}} \frac{\Delta_g}{1-\xi^2}, \quad (30)$$

where Θ_ξ is given in (13). This equation can be easily integrated and the solution for $a < 0$ and $D > 0$ is given by

$$\varphi(\gamma) = \frac{1}{2} \left(I_+ + I_- \right) \Big|_{\xi_{\text{in}}}^{\xi(\gamma)} + \varphi_{\text{in}}, \quad (31)$$

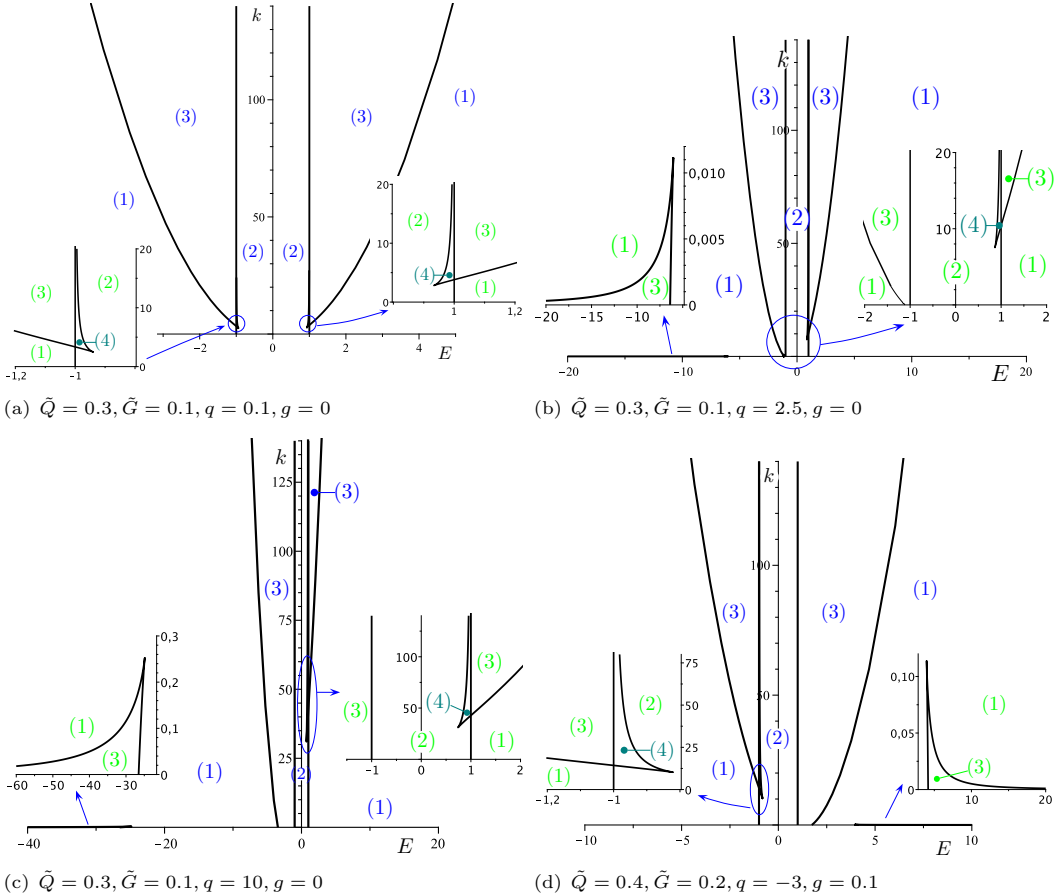


Figure 1: Parametric k - E diagrams showing the location of the regions (1)–(4), which reflect the number of zeros of the polynomial R in Eq. (11). Each region contains a set of orbits peculiar to it which are described in Table 1 and in the text (Section 3.2.2). Here the influence of the variation of the electric charge q of a test particle on the zeros of R is presented. Increasing the positive value of the electric charge in plots (a)–(c) one observes, that the region (4) with four positive zeros for negative E (left side) disappears slowly. When the sign of q is changed (along with the sign of g) the right and left side of the k - E diagrams are mirrored (compare plot (d) with the rest). One finds similar k - E diagrams by varying the value of the magnetic charge g . Because of the inequalities (14) the constant $k = K + \tilde{L}^2$ is positive.

where

$$I_{\pm} = -\frac{\tilde{L} \pm \Delta_g}{|\tilde{L} \pm \Delta_g|} \arcsin \frac{k + \kappa - (\tilde{L} \pm \Delta_g)^2 \mp (k + \kappa + (\tilde{L} \pm \Delta_g)^2) \xi}{\sqrt{D}(\xi \mp 1)} \quad (32)$$

For the special case $k = \tilde{L}^2$ and $\tilde{L} = \pm \Delta_g$ the solution reduces to the simple form

$$\varphi(\gamma) = \frac{1}{2} \frac{\tilde{L}}{|\tilde{L}|} \arcsin \frac{1 \pm 3\xi}{\xi \mp 1} \Big|_{\xi_{\text{in}}}^{\xi(\gamma)} + \varphi_{\text{in}} . \quad (33)$$

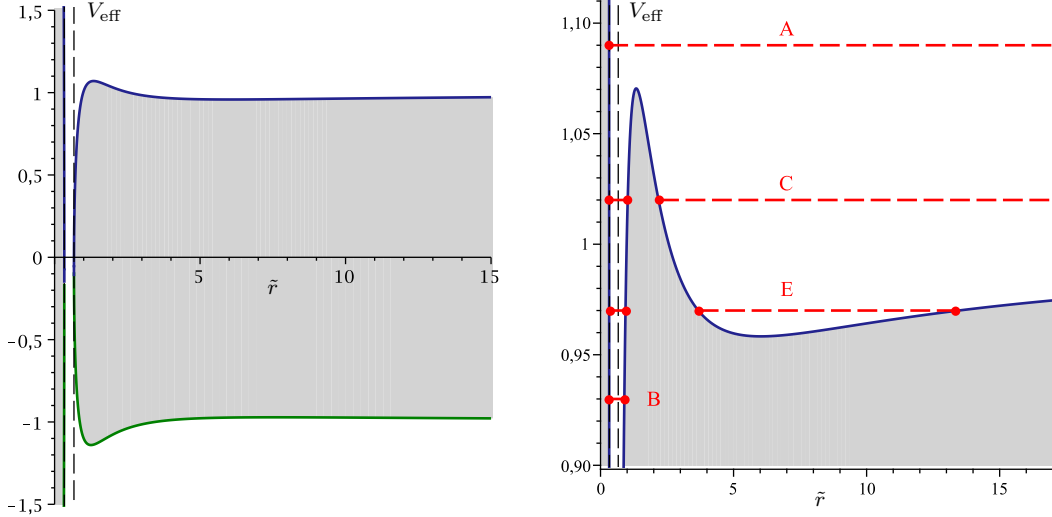
4.4 Solution of the \tilde{t} -equation

Eq. (10) consists of two \tilde{r} -integrals:

$$\tilde{t} - \tilde{t}_{\text{in}} = E \int_{\tilde{r}_{\text{in}}}^{\tilde{r}(\gamma)} \frac{\tilde{r}^4}{\tilde{\Delta}_r} \frac{d\tilde{r}}{\sqrt{R}} + \Delta_q \int_{\tilde{r}_{\text{in}}}^{\tilde{r}(\gamma)} \frac{\tilde{r}^3}{\tilde{\Delta}_r} \frac{d\tilde{r}}{\sqrt{R}} =: I_{\tilde{r}}^1(\gamma) + I_{\tilde{r}}^2(\gamma) . \quad (34)$$

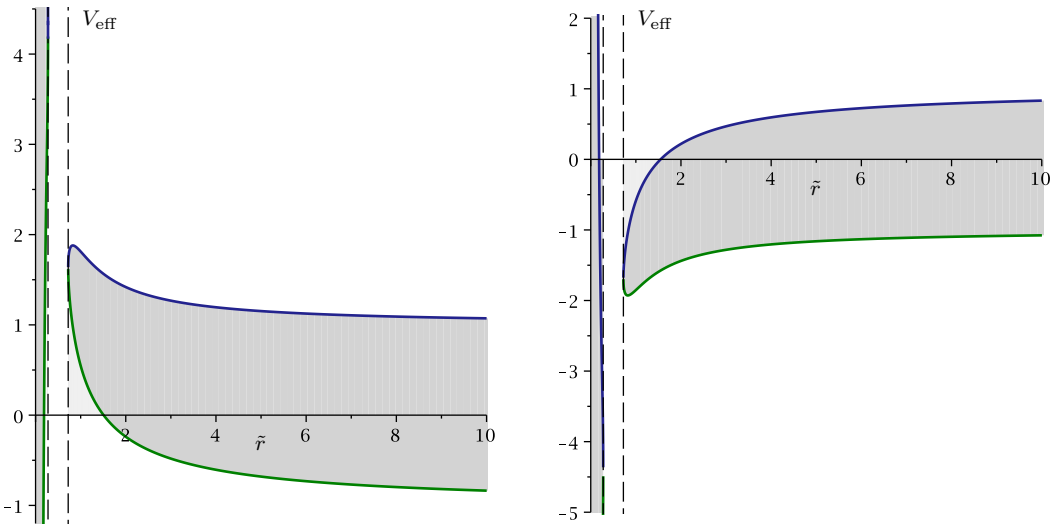
Consider $I_{\tilde{r}}^1$. The substitution $\tilde{r} = \pm \frac{b_3}{4y - \frac{b_2}{3}} + \tilde{r}_R$ reexpresses $I_{\tilde{r}}$ in terms of y :

$$I_{\tilde{r}}^1(\gamma) = E \int_{y_{\text{in}}}^y \mp \frac{dy}{\sqrt{P_3(y)}} \frac{(\tilde{r}_R (4y - \frac{b_2}{3}) \pm b_3)^4}{(4y - \frac{b_2}{3})^2 \Delta_y} , \quad (35)$$



(a) $\tilde{Q} = 0.4$, $\tilde{G} = 0.25$, $q = 0.05$, $g = 0.1$, $k = 4$:
Effective potential with four extrema.

(b) Detail of figure (a): 1 to 4 turning points are possible.
 V_{eff}^{\pm} for orbits of type A, B, C, E from Table 1 showing
the position of the orbit types BO, MBO, EO, TEO.
The points indicate the turning points of the motion
and the red horizontal dashed lines correspond to the
values of the energy E .



(c) $\tilde{Q} = 0.4$, $\tilde{G} = 0.2$, $q = -3$, $g = 0.1$, $k = 1$.

(d) $\tilde{Q} = 0.4$, $\tilde{G} = 0.2$, $q = 3$, $g = 0.1$, $k = 1$.

Figure 2: Effective potential $V_{\text{eff}}^{\pm}(\tilde{r})$ for different values of \tilde{Q} , \tilde{G} , q , g and k . The blue line represents V_{eff}^+ , the green line represents V_{eff}^- . The two potential parts glue at the horizons—glue points—with the ordinate $V_{\text{eff}}^{\pm}(r_{\pm}) = -\frac{\Delta q}{r_{\pm}}$. The grey area marks a physically forbidden zone. The positions of the horizons are shown by vertical dashed lines. At infinity the effective potential tends to the limiting values $\lim_{\tilde{r} \rightarrow \infty} V_{\text{eff}}^{\pm} = \pm 1$. Figures (c) and (d) are plotted for opposite electric charges of the test particle. The glue points of the V_{eff}^{\pm} are either positive (for $q < 0$) or negative (for $q > 0$). As can be seen from the k - E diagram in Fig. 1(d) there are regions with 1, 2 or 3 zeros for the potential (c) with $k = 1$.

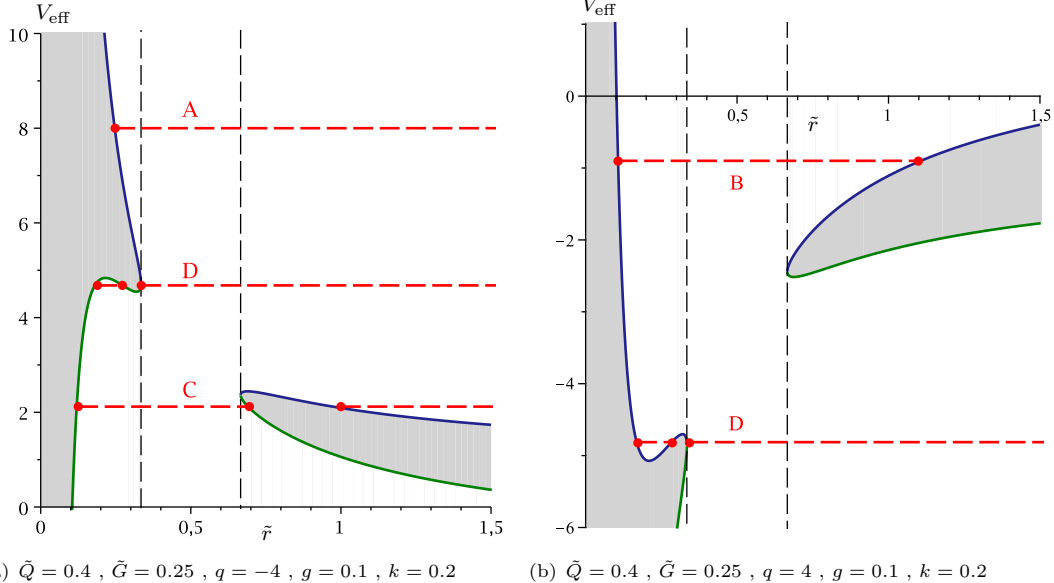


Figure 3: Effective potential $V_{\text{eff}}^{\pm}(\tilde{r})$ for different values of \tilde{Q} , \tilde{G} , q , g and k . The grey area marks a physically forbidden zone. In this case up to 3 turning points exist for $\tilde{r} \leq \tilde{r}_-$. Such an effect can be caused by a high charge of the test particle. In the plot (a) the orbits of type A, C, D from Table 1 are shown.

where $\Delta_y = \tilde{\Delta}_r(\tilde{r}_R) \left(4y - \frac{b_2}{3}\right)^2 \pm (2\tilde{r}_R - 1)b_3 \left(4y - \frac{b_2}{3}\right) + b_3^2 = 16\tilde{\Delta}_r(\tilde{r}_R)(y - p_1)(y - p_2)$. Here, p_1 and p_2 are two zeros of Δ_y .

We next apply a partial fractions decomposition upon Eq. (35)

$$I_{\tilde{r}}^1(\gamma) = E \int_{\gamma_{\text{in}}}^{\gamma} \mp \frac{dy}{\sqrt{P_3(y)}} \left(K_0 + \sum_{j=1}^3 \frac{K_j}{y - p_j} + \frac{K_4}{(y - p_3)^2} \right), \quad (36)$$

where $p_3 = \frac{b_2}{12}$ and K_i , $i = 0, \dots, 4$, are constants which arise from the partial fractions decomposition. These depend on the parameters of the metric and the test particle and on \tilde{r}_R . After the substitution $y = \wp(v)$ with $\wp'(v) = (-1)^\rho \sqrt{4\wp^3(v) - g_2\wp(v) - g_3}$, where ρ is either 0 or 1 depending on the sign of $\wp'(v)$ in the considered interval and on the branch of the square root, Eq. (36) simplifies to

$$I_{\tilde{r}}^1(\gamma) = \mp E \int_{v_{\text{in}}}^v (-1)^\rho \left(K_0 + \sum_{j=1}^3 \frac{K_j}{\wp(v) - p_j} + \frac{K_4}{(\wp(v) - p_3)^2} \right) dv. \quad (37)$$

Here $v = v(\gamma) = \gamma - \gamma'_{\text{in}}$ and $v_{\text{in}} = v(\gamma_{\text{in}})$.

The second integral $I_{\tilde{r}}^2$ in (34) can be reduced in a similar way to the necessary form, yielding:

$$I_{\tilde{r}}^2(\gamma) = \mp \Delta_q \int_{v_{\text{in}}}^v (-1)^\rho \left(H_0 + \sum_{j=1}^3 \frac{H_j}{\wp(v) - p_j} \right) dv, \quad (38)$$

where H_i , $i = 0, \dots, 3$, are constants which arise from the partial fractions decomposition.

The final solution takes the form (details can be found in the appendices A and B)

$$\begin{aligned} I_{\tilde{r}}(\gamma) &= \mp(-1)^\rho E \left\{ (K_0 + A_2 K_4) (v - v_{\text{in}}) + \sum_{i=1}^2 \left[\sum_{j=1}^3 \frac{K_j}{\wp'(v_{ji})} \left(\zeta(v_{ji})(v - v_{\text{in}}) + \log \frac{\sigma(v - v_{ji})}{\sigma(v_{\text{in}} - v_{ji})} \right) \right. \right. \\ &\quad \left. \left. - \frac{K_4}{(\wp'(v_{3i}))^2} \left(\zeta(v - v_{3i}) - \zeta(v_{\text{in}} - v_{3i}) + \frac{\wp''(v_{3i})}{\wp'(v_{3i})} \log \frac{\sigma(v - v_{3i})}{\sigma(v_{\text{in}} - v_{3i})} \right) \right] \right\} \\ &\quad \mp(-1)^\rho \Delta_q \left\{ H_0 (v - v_{\text{in}}) + \sum_{i=1}^2 \left[\sum_{j=1}^3 \frac{H_j}{\wp'(v_{ji})} \left(\zeta(v_{ji})(v - v_{\text{in}}) + \log \frac{\sigma(v - v_{ji})}{\sigma(v_{\text{in}} - v_{ji})} \right) \right] \right\}, \end{aligned} \quad (39)$$

where v_{ji} are the poles of the functions $(\wp(v) - p_j)^{-1}$ and $(\wp(v) - p_3)^{-2}$ in (36) such that $\wp(v_{j1}) = p_j = \wp(v_{j2})$ since $\wp(v)$ is an even elliptic function of order two which assumes every value in the fundamental

parallelogram with multiplicity two. Here $\zeta(v)$ is the Weierstraß zeta function and $\sigma(v)$ is the Weierstraß sigma function [26]; $A_2 = -\sum_{i=1}^2 \left(\frac{\wp(v_{3i})}{(\wp'(v_{3i}))^2} + \frac{\wp''(v_{3i})\zeta(v_{3i})}{(\wp'(v_{3i}))^3} \right)$ is a constant.

4.5 The orbits

With these analytical results we have found the complete set of orbits for massive charged particles. The following figures show solutions of the geodesic equations for the spatial coordinates. We start with small charges of a test particle in Figs. 4, 5, 6. The orbits here lie on cones with large opening angle $\Delta\vartheta \rightarrow \pi$. Depending on the energy of the test particle one gets MBO, BO, TEO or EO. In all these figures the energy is chosen in the vicinity of the maximum of the effective potential.

In the Figs. 7, 8, 9 we increased the charge of the test particle. The orbital cone is most evident here. The orbit 7(a) with its x - z projection (b) is of type D from Table 1. The test particle orbits the singularity at $\tilde{r} = 0$. Such kinds of orbits are peculiar to particles with large charge (and small constant k). An example of the effective potential is presented in Fig. 3. As compared to *super test particles* with small mass and small charge, a particle with small mass and large charge is not *super* any more, but it may still be regarded as a *test body* or *test particle* [27].

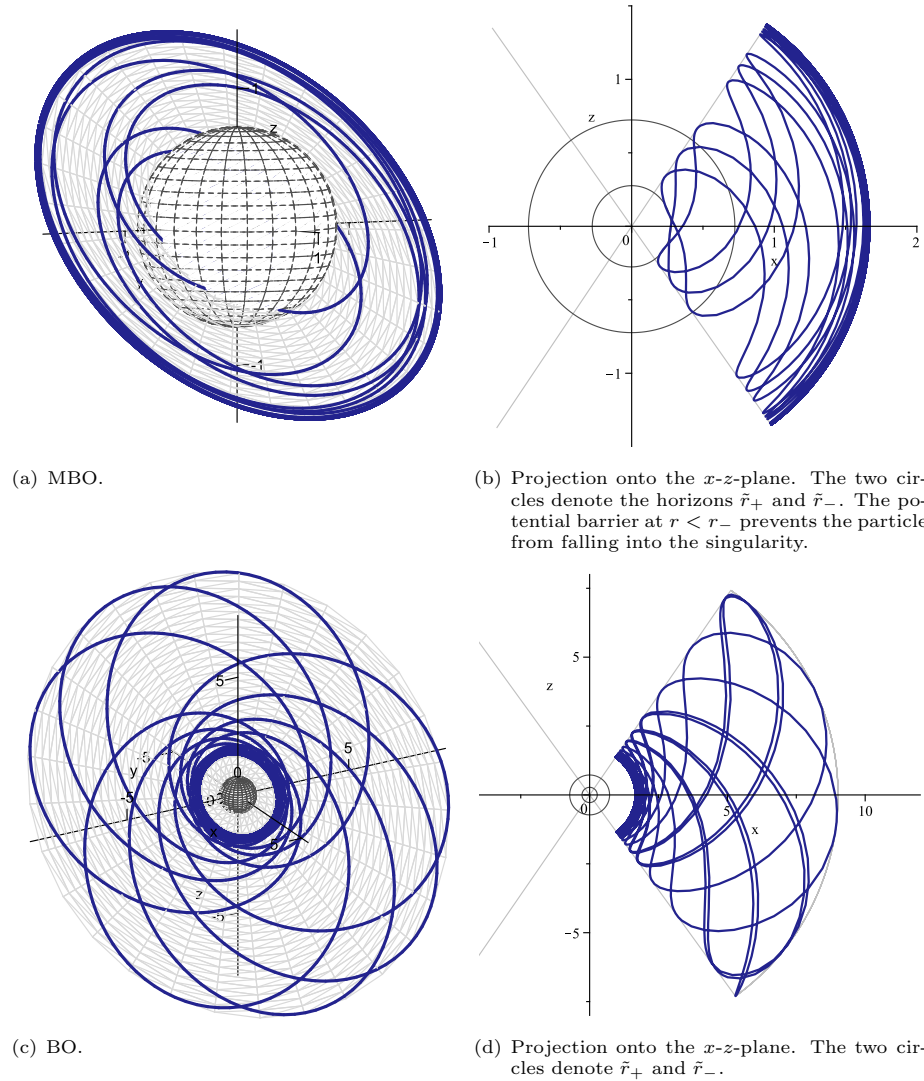
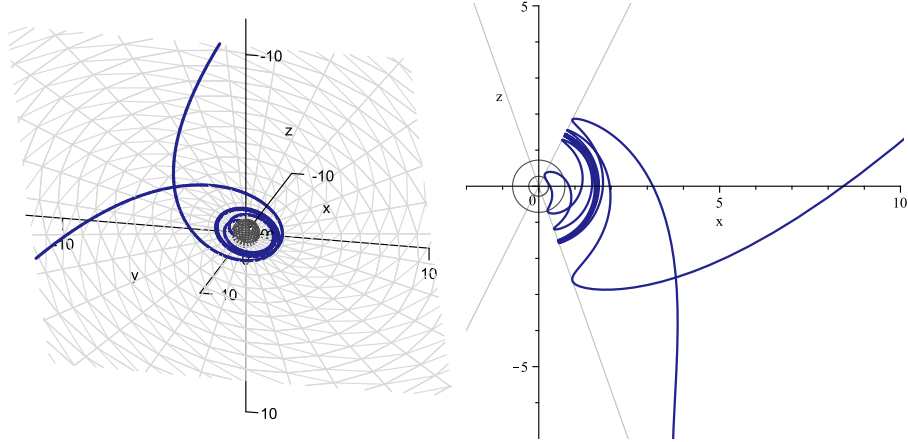


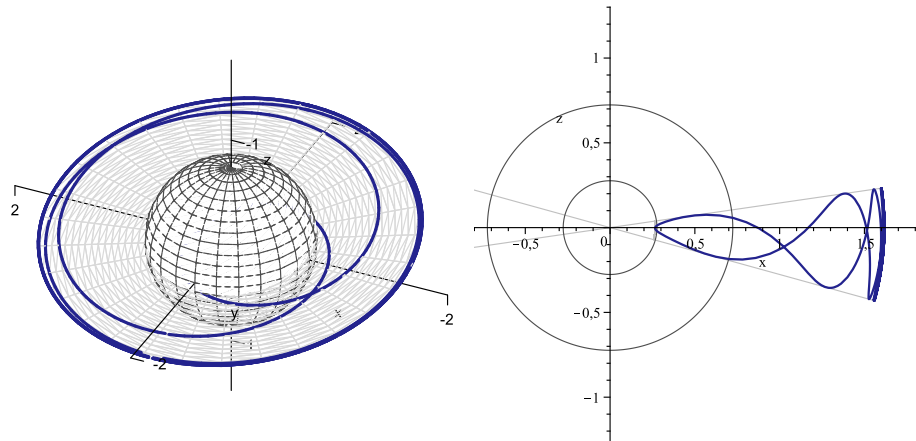
Figure 4: MBO and BO with parameters $\tilde{Q} = 0.4$, $\tilde{G} = 0.2$, $q = 0.1$, $g = 0.1$, $k = 3$, $E = 0.9548$, $\tilde{L} = 1.0$. The sphere in the 3d plots shows the horizon \tilde{r}_+ . Orbit lie on cones with large opening angle $\Delta\vartheta \rightarrow \pi$.



(a) TEO. The sphere shows the horizon \tilde{r}_+ .

(b) Projection onto the x - z -plane. The two circles denote \tilde{r}_+ and \tilde{r}_- .

Figure 5: TEO with parameters $\tilde{Q} = 0.4$, $\tilde{G} = 0.2$, $q = 1.0$, $g = 0.1$, $k = 6.5$, $E = 1.0039$, $\tilde{L} = 1.0$. The particle crosses both horizons, is reflected at the potential barrier and emerges into a second universe, where it moves out to infinity. The orbit lies on a cone with large opening angle $\Delta\vartheta \rightarrow \pi$.



(a) MBO.

(b) Projection onto the x - z -plane. The two circles denote the horizons \tilde{r}_+ and \tilde{r}_- . The potential barrier at $r < r_-$ prevents the particle from falling into the singularity.

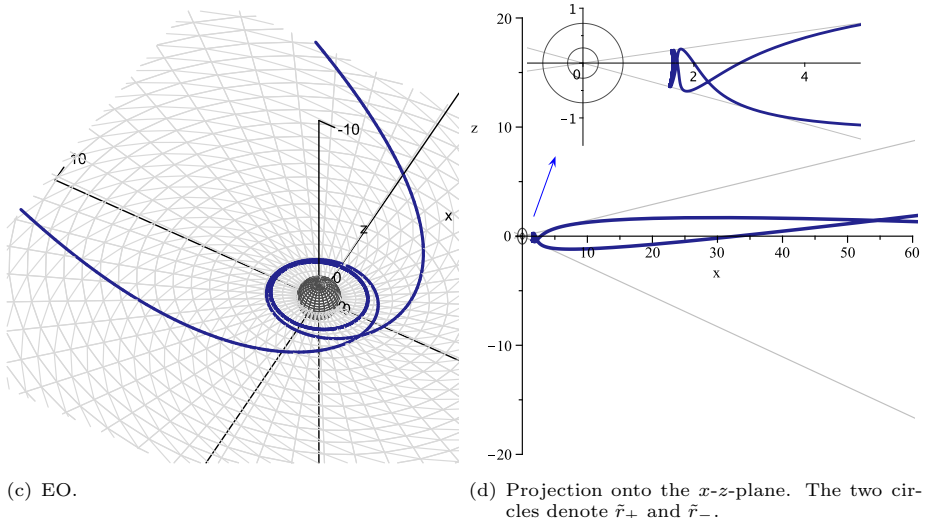
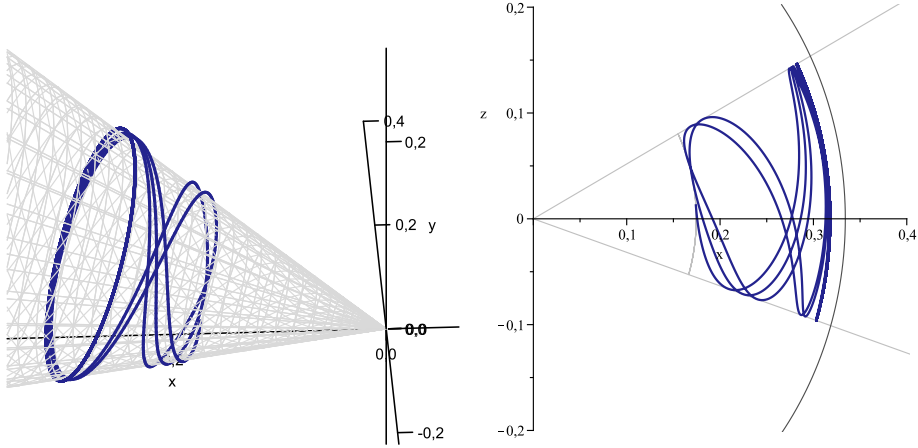
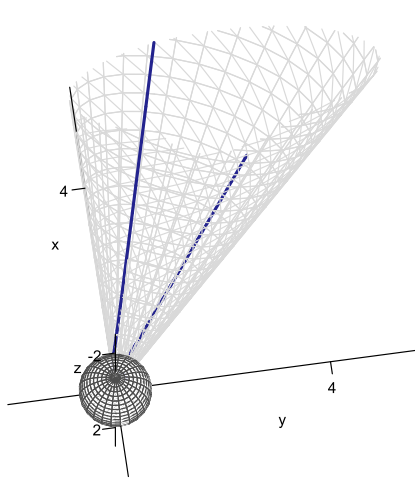


Figure 6: MBO and EO with parameters $\tilde{Q} = 0.4$, $\tilde{G} = 0.2$, $q = 1.0$, $g = 0.1$, $k = 6.5$, $E = 1.0038$, $\tilde{L} = 2.5$. An increase of \tilde{L} (compare e.g. with Fig. 5(b)) leads to a decrease of the opening angles of the two cones, which confine the orbit. The orbits lie on cones with large opening angle $\Delta\vartheta \rightarrow \pi$.

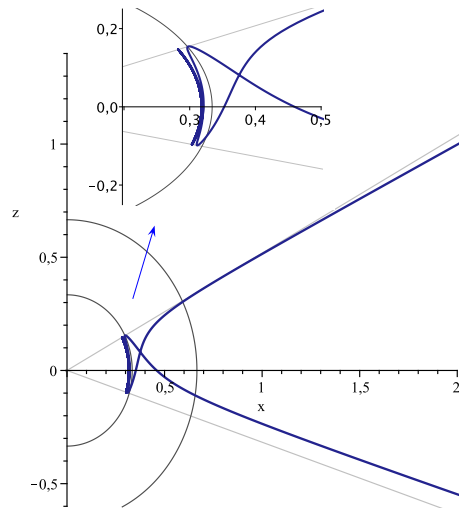


(a) BO. The orbit lies on a cone behind the inner horizon. For this orbit the singularity is not hidden.

(b) Projection onto the x - z -plane. The part of the black circle is the horizon \tilde{r}_- . Here $r_1, r_2 < \tilde{r}_-$.

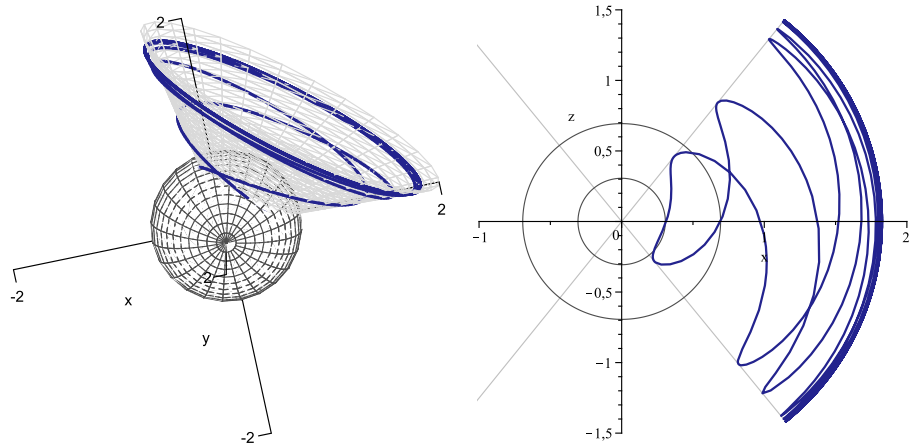


(c) TEO



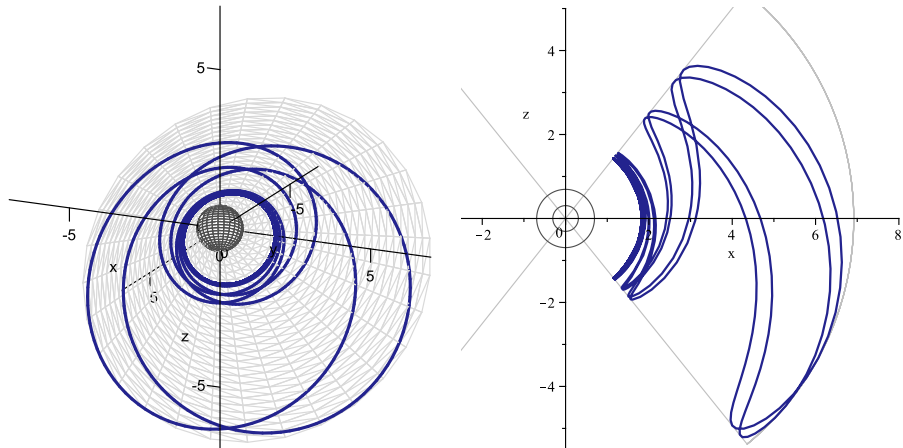
(d) Projection onto the x - z -plane. The two circles denote the horizons \tilde{r}_+ and \tilde{r}_- .

Figure 7: BO and TEO with parameters $\tilde{Q} = 0.4$, $\tilde{G} = 0.25$, $q = -4$, $g = 0.2$, $k = 0.2$, $E = 4.4673$, $\tilde{L} = 0.1$. Because of the large charge of the test particle the orbital cone has a small opening angle.



(a) MBO.

(b) Projection onto the x - z -plane. The two circles denote the horizons \tilde{r}_+ and \tilde{r}_- . The potential barrier at $r < r_-$ prevents the particle from falling into the singularity.



(c) BO.

(d) Projection onto the x - z -plane. The two circles denote the horizons \tilde{r}_+ and \tilde{r}_- .

Figure 8: MBO and BO with parameters $\tilde{Q} = 0.45$, $\tilde{G} = 0.1$, $q = 0.0$, $g = 4.0$, $k = 5$, $E = 0.9167$, $\tilde{L} = 0.01$. The sphere in the 3d plots shows the horizon \tilde{r}_+ .

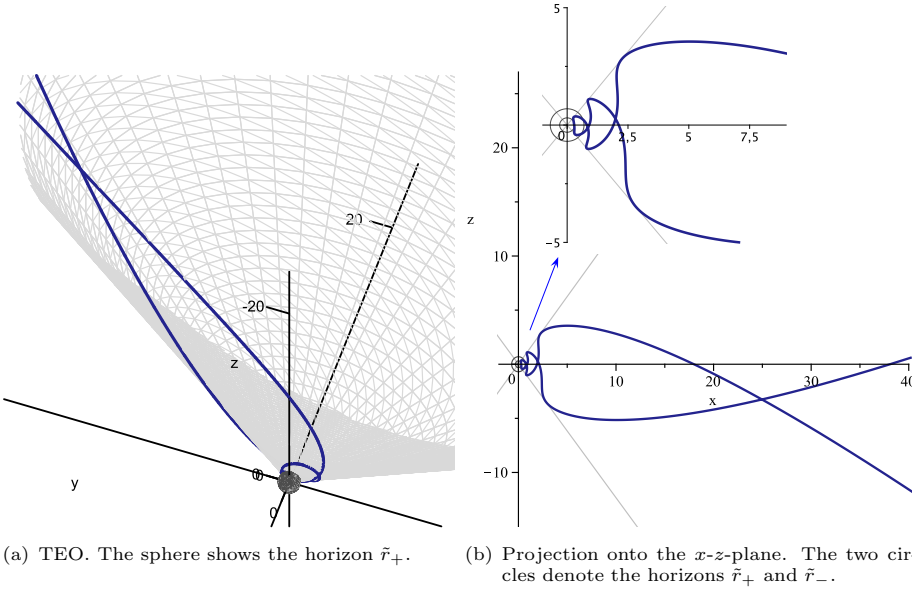


Figure 9: TEO with parameters $\tilde{Q} = 0.45$, $\tilde{G} = 0.1$, $q = 0.0$, $g = 4.0$, $k = 5.0$, $E = 1.0001$, $\tilde{L} = 0.01$. The particle crosses both horizons, is reflected at the potential barrier and emerges into a second universe, where it moves out to infinity.

4.6 The observables

The Reissner-Nordström space-time is believed to be of little astrophysical relevance, because a charged black hole would lose its charge quickly by interactions with matter around it. Nevertheless, the study of charged black holes can help to understand more general space-times with sources immersed into spherically symmetric matter backgrounds.

For test particle motion one can define frame independent observables such as the perihelion shift for bound orbits, the light deflection for escape orbit, the deflection angle for flyby orbits, or the Lense-Thirring effect. We follow the lines of [12] to calculate possible observables.

We consider here bound orbits of type E and D from the Table 1. The \tilde{r} -motion is periodic with a period

$$\omega_{\tilde{r}} = 2 \int_{r_{\min}}^{r_{\max}} \frac{d\tilde{r}}{\sqrt{R}} = 2 \int_{e_1}^{e_2} \frac{dy}{\sqrt{P_3(y)}}, \quad (40)$$

where e_1 and e_2 are the zeros of $P_3(y)$ related to r_{\min} and r_{\max} . The corresponding orbital frequency is $\frac{2\pi}{\omega_{\tilde{r}}}$.

The period of the ϑ -motion is given by

$$\omega_{\vartheta} = 2 \int_{\vartheta_{\min}}^{\vartheta_{\max}} \frac{d\vartheta}{\sqrt{\Theta}} = -2 \int_{\xi_{\max}}^{\xi_{\min}} \frac{d\xi}{\sqrt{\Theta_{\xi}}} = \frac{2\pi}{\sqrt{-a}}, \quad (41)$$

and the corresponding frequency by $\frac{2\pi}{\omega_{\vartheta}}$.

The secular accumulation rates of the angle φ and the time t are given by:

$$Y_{\varphi} = \frac{2}{\omega_{\vartheta}} \int_{\xi_{\max}}^{\xi_{\min}} \frac{\tilde{L} + \Delta g \xi}{1 - \xi^2} \left(-\frac{d\xi}{\sqrt{\Theta_{\xi}}} \right) = \frac{1}{\omega_{\vartheta}} (I_+ + I_-)|_{\xi_{\max}}^{\xi_{\min}} = \sqrt{-a}. \quad (42)$$

and

$$\begin{aligned} \Gamma &= \frac{2}{\omega_{\tilde{r}}} \left(E \int_{r_{\min}}^{r_{\max}} \frac{\tilde{r}^4}{\tilde{\Delta}_r} \frac{d\tilde{r}}{\sqrt{R}} + \Delta_q \int_{r_{\min}}^{r_{\max}} \frac{\tilde{r}^3}{\tilde{\Delta}_r} \frac{d\tilde{r}}{\sqrt{R}} \right) \\ &= \frac{2}{\omega_{\tilde{r}}} \left(I_{\tilde{r}}^1|_{\gamma_{e_1}}^{\gamma_{e_2}} + I_{\tilde{r}}^2|_{\gamma_{e_1}}^{\gamma_{e_2}} \right), \end{aligned} \quad (43)$$

where $I_{\tilde{r}}^1$ and $I_{\tilde{r}}^2$ defined in the equations (37) and (38) are evaluated at γ_{e_i} corresponding to the root e_i , $i = 1, 2$. The orbital frequencies Ω_r , Ω_{ϑ} and Ω_{φ} are then given by:

$$\Omega_{\tilde{r}} = \frac{2\pi}{\omega_{\tilde{r}}} \frac{1}{\Gamma}, \quad \Omega_{\vartheta} = \frac{2\pi}{\omega_{\vartheta}} \frac{1}{\Gamma}, \quad \Omega_{\varphi} = \frac{Y_{\varphi}}{\Gamma}. \quad (44)$$

The perihelion shift and the Lense–Thirring effects are defined as differences between these orbital frequencies

$$\Delta_{\text{perihelion}} = \Omega_\varphi - \Omega_{\tilde{r}} = \left(\sqrt{-a} - \frac{2\pi}{\omega_{\tilde{r}}} \right) \frac{1}{\Gamma} \quad (45)$$

$$\Delta_{\text{Lense–Thirring}} = \Omega_\varphi - \Omega_\vartheta = 0 . \quad (46)$$

As expected, there is no Lense–Thirring effect.

5 Conclusions and Outlook

In this paper we presented the analytic solution of the geodesic equations of charged test particles in the Reissner-Nordström space-time in terms of the Weierstraß \wp , σ and ζ functions. The derived orbits depend on the particle's energy, angular momentum, electric and magnetic charges, Carter constant and on the parameters of the gravitating and charged source. We discussed the general structure of the orbits and gave a complete classification of their types. The orbits of charged test particles lie on a cone similar to the motion in Taub-NUT space-times with gravitomagnetic charge. This happens because of the non-vanishing $\Delta_g \cos \vartheta$ term in the equations (8) and (9). Thus, the motion of only electrically charged particles around an only electrically charged source or the motion of only magnetically charged particles around an only magnetically charged source reduces to motion in a plane. However, this is not true for the motion of test particles with both types of charge around a charged source or the motion of charged particles around a source with both types of charges (as in the examples considered in this paper).

We showed that for large charge of test particles bound orbits behind the inner horizon are possible. So, a test particle moves in a space-time, that has horizons which hide the singularity, but for the motion of the particle the singularity is not hidden. Such an effect is not present for neutral particles.

Finally we remark, that as compared to the geodesics in the field of a gravitomagnetic monopole [12], the geodesics in the Reissner-Norström space-time are complete, because the space-time can be analytically continued (without destroying some of its essential properties [16]). Thus at least theoretically, a particle crossing the horizons may emerge afterwards into another universe, following a many-world orbit.

Acknowledgement

We would like to thank Jutta Kunz and Claus Lämmerzahl for suggesting this research topic and for helpful discussions and interesting remarks. We also acknowledge fruitful discussions with Eva Hackmann. V.K. acknowledges financial support of the German Research Foundation DFG.

A Integration of elliptic integrals of the third kind

We consider an integral of the type $I_1 = \int_{v_{\text{in}}}^v \frac{dv}{\wp(v) - p_1}$. This integral is of the third kind because the function $f_1(v) = (\wp(v) - p_1)^{-1}$ has two simple poles v_1 and v_2 in a fundamental parallelogram with vertices $0, 2\omega_1, 2\omega_1 + 2\omega_2, 2\omega_2$, where $2\omega_1$ and $2\omega_2$ are fundamental periods of $\wp(v)$ and $\wp'(v)$.

Consider the Laurent series for the function f_1 around v_i

$$f_1(v) = a_{-1,i}(v - v_i)^{-1} + \text{holomorphic part} , \quad (47)$$

and the Taylor series of f_1^{-1} about v_i

$$f_1^{-1}(v) = \wp'(v_i)(v - v_i) + \mathcal{O}(v^2) . \quad (48)$$

Comparing the coefficients in the equality $1 = f_1(v)f_1^{-1}(v)$ where

$$1 = f_1(v) (\wp'(v_i)(v - v_i) + \mathcal{O}(v^2)) = a_{-1,i}\wp'(v_i) + \mathcal{O}(v^2) \quad (49)$$

yields $a_{-1,i} = \frac{1}{\wp'(v_i)}$. Thus, the function $f_1(v)$ has a residue $\frac{1}{\wp'(v_i)}$ in v_i .

The Weierstraß $\zeta(v)$ function is an elliptic function with a simple pole in 0 and residue 1. Then the function $A_1 = f_1(v) - \sum_{i=1}^2 \frac{\zeta(v-v_i)}{\wp'(v_i)}$ is an elliptic function without poles and therefore a constant [26], which can be determined from $f_1(0) = 0$. Thus,

$$f_1(v) = \sum_{i=1}^2 \frac{\zeta(v-v_i) + \zeta(v_i)}{\wp'(v_i)}, \quad (50)$$

here $\wp'(v_2) = \wp'(2\omega_j - v_1) = -\wp'(v_1)$. Applying now the definition of the Weierstraß σ -function $\int_{v_{\text{in}}}^v \zeta(v)dv = \log \sigma(v) - \log \sigma(v_{\text{in}})$ upon the integral I_1 we get the solution

$$I_1 = \int_{v_{\text{in}}}^v f_1(v)dv = \sum_{i=1}^2 \frac{1}{\wp'(v_i)} \left(\zeta(v_i)(v - v_{\text{in}}) + \log \frac{\sigma(v - v_i)}{\sigma(v_{\text{in}} - v_i)} \right). \quad (51)$$

B Integration of elliptic integrals of the type $I_2 = \int_{v_{\text{in}}}^v \frac{dv}{(\wp(v) - p_3)^2}$

We consider the Laurent series of $f_2(v)$ and the Taylor series of $f_2^{-1}(v)$ around v_i for $f_2(v) = \frac{1}{(\wp(v) - p_3)^2}$:

$$f_2(v) = a_{-2,i}(v - v_i)^{-2} + a_{-1,i}(v - v_i)^{-1} + \text{holomorphic part}, \quad (52)$$

$$\begin{aligned} f_2^{-1}(v) &= \left(\wp'(v_i)(v - v_i) + \frac{1}{2}\wp''(v_i)(v - v_i)^2 + \mathcal{O}(v^3) \right)^2 \\ &= (\wp'(v_i))^2(v - v_i)^2 + \wp'(v_i)\wp''(v_i)(v - v_i)^3 + \mathcal{O}(v^4). \end{aligned} \quad (53)$$

The function $f_2(v)$ has poles of second order in v_1 and v_2 such that $f_2(v_1) = p_3 = f_2(v_2)$. Comparison of the coefficients in

$$\begin{aligned} 1 &= f_2(v) \left((\wp'(v_i))^2(v - v_i)^2 + \wp'(v_i)\wp''(v_i)(v - v_i)^3 + \mathcal{O}(v^4) \right) \\ &= a_{-2,i}(\wp'(v_i))^2 + (v - v_i) \left[a_{-1,i}(\wp'(v_i))^2 + a_{-2,i}\wp'(v_i)\wp''(v_i) \right] + \mathcal{O}(v^2) \end{aligned} \quad (54)$$

yields

$$a_{-2,i} = \frac{1}{(\wp'(v_i))^2}, \quad a_{-1,i} = -\frac{\wp''(v_i)}{(\wp'(v_i))^3}. \quad (55)$$

The function $\wp(v)$ possesses a pole of second order in $v = 0$ with residuum 0 and the Laurent series of \wp begins with v^{-2} . Then the Laurent series of $a_{-2,i}\wp(v - v_i)$ around v_i begins with $a_{-2,i}(v - v_i)^{-2}$ which is similar to the first term in (52). The Laurent series of $a_{-1,i}\zeta(v - v_i)$ around v_i begins with $a_{-1,i}(v - v_i)^{-1}$.

Thus, the function $A_2 = f_2(v) - \sum_{i=1}^2 \left(\frac{\wp(v - v_i)}{(\wp'(v_i))^2} - \frac{\wp''(v_i)\zeta(v - v_i)}{(\wp'(v_i))^3} \right)$ has no poles and is constant [26] and

can be calculated from $f_2(0) = 0$: $A_2 = -\sum_{i=1}^2 \left(\frac{\wp(v_i)}{(\wp'(v_i))^2} + \frac{\wp''(v_i)\zeta(v_i)}{(\wp'(v_i))^3} \right)$.

Using of $\int_{v_{\text{in}}}^v \wp(v)dv = -\zeta(v) + \zeta(v_{\text{in}})$ and the definition of the σ -function the integral I_2 takes the form:

$$I_2 = \int_{v_{\text{in}}}^v f_2(v)dv = A_2(v - v_{\text{in}}) - \sum_{i=1}^2 \left[\zeta(v - v_i) - \zeta(v_{\text{in}} - v_i) + \frac{\wp''(v_i)}{\wp'(v_i)} \log \frac{\sigma(v - v_i)}{\sigma(v_{\text{in}} - v_i)} \right] \frac{1}{(\wp'(v_i))^2}. \quad (56)$$

References

- [1] J. F. Plebański and M. Demiański *Ann. Phys.* (N.Y.), **98**, 98 (1976)
- [2] Griffiths J B and Podolsky J 2006, *Int. J. Mod. Phys.* **15** 335
- [3] F. R. Tangherlini, *Nuovo Cim.*, **27**, 636 (1963).

- [4] Y. Hagiwara, *Japan. J. Astron. Geophys.* **8**, 67 (1931).
- [5] S. Chandrasekhar, *The Mathematical Theory of Black Holes* (Oxford University Press, Oxford 1983)
- [6] V. F. Gackstatter, *Ann. der Phys.* **40**, 352 (1983).
- [7] J. Bičák, Z. Stuchlík, V. Balek, *Bull. Astron. Inst. Czechosl.* **40**, 65 (1989).
- [8] D. Bini, C. Cherubini, R.T. Jantzen, and B. Mashhoon, *Class. Quantum Grav.* **20** 457 (2003)
- [9] E. Hackmann and C. Lämmerzahl, *Phys. Rev. Lett.* **100**, 171101 (2008).
- [10] E. Hackmann and C. Lämmerzahl, *Phys. Rev. D* **78**, 024035 (2008).
- [11] E. Hackmann, V. Kagramanova, J. Kunz and C. Lämmerzahl, *Phys. Rev. D* **78** 124018 (2008)
- [12] V. Kagramanova, J. Kunz, E. Hackmann and C. Lämmerzahl, *Phys. Rev. D* **81** 124044 (2010)
- [13] E. Hackmann, C. Lämmerzahl, V. Kagramanova and J. Kunz, *Phys. Rev. D* **81** 044020 (2010)
- [14] E. Hackmann, V. Kagramanova, J. Kunz and C. Lämmerzahl, *Europhys. Lett.* **88** 30008 (2009)
- [15] N. Straumann, *General Relativity: With Applications To Astrophysics*, Springer, Berlin (2004)
- [16] J. G. Miller, M. D. Kruskal and B. Godfrey, *Phys. Rev. D* **4** 2945 (1971)
- [17] Y. Mino, *Phys. Rev. D* **67** 084027 (2003)
- [18] V. L. Golo, *Pis'ma Zh. Eksp. Teor. Fiz.* **35** 535 (1982)
- [19] J. Sivardiére, *Eur. J. Phys.* **21** 183 (2000)
- [20] C. W. Misner and A. H. Taub, *Sov. Phys. JETP* **28** 122 (1969); *Zh. Eksp. Teor. Fiz.* **55** 233 (1968)
- [21] R. L. Zimmerman and B. Y. Shahir, *Gen. Rel. Grav.* **21** 821 (1989)
- [22] D. Lynden-Bell and M. Nouri-Zonos, *Rev. Mod. Phys.* **70** 427 (1998)
- [23] D. Christodoulou and R. Ruffini, *Phys. Rev. D* **4**, 3552 (1971).
- [24] G. Denardo and R. Ruffini, *Phys. Lett.* **45 B**, 260 (1973)
- [25] N. Deruelle and R. Ruffini, *Phys. Lett.* **52 B**, 437 (1974).
- [26] A. I. Markushevich, *Theory of functions of a complex variable*, Vol. III, Prentice-Hall, Inc., Englewood Cliffs, N.J. (1967)
- [27] W. A. Hiscock, *Ann. Phys.* **131** 245 (1981)
- [28] V. Kagramanova, J. Kunz, C. Lämmerzahl, *Class. Quantum Grav.* **25** 105023 (2008)